Nonlocal elasticity in plates using novel trial functions

Sh. Faroughi , S.M.H. Goushegir , H. Haddad Khodaparast , M.I. Friswell

PII: S0020-7403(16)30815-3
DOI: 10.1016/j.ijmecsci.2017.05.034
Reference: MS 3713

To appear in: *International Journal of Mechanical Sciences*

Received date: 17 November 2016
Revised date: 29 April 2017
Accepted date: 28 May 2017

Please cite this article as: Sh. Faroughi , S.M.H. Goushegir , H. Haddad Khodaparast , M.I. Friswell , Nonlocal elasticity in plates using novel trial functions, *International Journal of Mechanical Sciences* (2017), doi: 10.1016/j.ijmecsci.2017.05.034

Highlights

- The Ritz formulation using boundary characteristic orthogonal polynomials is proposed
- The method is efficient for solving non-local boundary-value problems is presented
- The nonlocal mass and stiffness matrices are independent of the mesh distribution.
- Several numerical examples are used to demonstrate the accuracy of the method.
- The method is compared against nonlocal finite-element method.

Nonlocal elasticity in plates using novel trial functions

Sh. Faroughi[1], S. M. H. Goushegir[1], H. Haddad Khodaparast[2], M.I. Friswell[2]

Faculty of Mechanical Engineering, Urmia University of Technology, Urmia, Iran

College of Engineering, Swansea University, Swansea, UK

Abstract

This study presents the Ritz formulation, which is based on boundary characteristic orthogonal polynomials (BCOPs), for the two-phase integro-differential form of the Eringen nonlocal elasticity model. This approach is named the nonlocal Ritz method (NL-RM). This feature greatly reduces the computational cost compared to the nonlocal finite-element method (NL-FEM). Another advantage of this approach is that, unlike NL-FEM, the nonlocal mass and stiffness matrices are independent of the mesh distribution. Here, these formulations are applied to study the static-bending and free-dynamic analyses of the Kirchhoff plate model. In this paper, novel 2D BCOPs of the plate are derived as coordinate functions. These polynomials are generated using a modified Gram-Schmidt process and satisfy the given geometrical boundary conditions as well as the natural boundary conditions. The accuracy and convergence of the presented model, demonstrated through several numerical examples, are discussed. A concise argument on the advantages of NL-RM compared to NL-FEM is also provided.

Keywords:

Two-phase integro-differential formulation, Ritz Method, Boundary characteristic orthogonal polynomials, Kirchhoff plate, static deflection, dynamic analysis

1. Introduction

The classical (local) continuum theories assume that the strain and stress at each point are related. However, these theories have been shown to be inadequate for numerous situations in which a characteristic length scale of the medium must be considered in the physical solution. The local theory cannot be used to describe the stress and strain fields around sharp crack tips, the dispersion of elastic waves, strain softening, size-dependent effects and dislocation (Bazant and Cedolin, 2010). As a result, nonlocal continuum theories are needed to model the structural responses of new materials to account for small-scale effects. Nonlocal theories assume that the stress at each point is affected by the strain at all points in the field. Kröner (1967), Kunin (1968), and Krumhansl (1968) proposed for the first time the idea of the nonlocal theory. Among size-dependent theories, one of the most well-known is the nonlocal continuum theory of Eringen. In this theory, the scale effect and long-range interatomic interactions are entered as material parameters into the constitutive equations. Later, Edelen and Laws (1971), Edelen et al. (1971), and Eringen and Edelen (1972) improved nonlocal formulations in a thermodynamic framework and accounted for long-range interactions in the constitutive equations in an integral form. Eringen (1987) and Altan (1989) presented the two-phase integro-differential nonlocal elasticity theory, which includes both local and nonlocal integral-type elasticity theories by assigning a volume fraction to each of the theories. In integral non-local theory, an integral operator is represented as a material parameter to take into account the nonlocal nature of the material structure. In this theory, the stress at a material point is dependent on a positive distance-decaying kernel function as a weighted integral of strains over a specified finite region. This theory for isotropic material results in a set of integro-partial differential equations for the displacement domain, which are difficult to solve, particularly for mixed boundary-value problems (Shaat, 2015).

The integral nonlocal elasticity theory was revised by Polizzotto (2001), who proposed nonlocal finite-element models to remove the difficulties of employing the nonlocal boundary conditions. Polizzotto (2001) obtained nonlocal finite element (NL-FEM) and an alternative FEM-based iterative formulation of the integral-type nonlocal model based on three variational principles. A nonlocal-type FEM (NL-FEM) was developed in which the symmetric global-stiffness

matrix includes the nonlocal characteristics of the problem. Moreover, an iterative-FE-based solution method (Iterative-FEM) was presented in which the local strain energy is iteratively corrected by an imposed correction strain. The NL-FEM may be used to solve one- and two-dimensional nonlocal elastic problems. Pisano and Fuschi (2003) investigated an elastic bar subjected to tension based on Eringen's nonlocal integral-type model by transforming the governing equation into the standard solvable Volterra integral equation of the second type. Later, Benvenuti and Simone (2013), proposed a closed-form solution of the local-nonlocal strain-stress law for a homogeneous rod subjected to different load cases by reducing the integro-differential boundary value problem to a differential one. An NL-FEM was developed, in detail, to solve 2D elastic problems (in-plane motion) for homogeneous (Pisano et al., 2009a) and non-homogeneous (Pisano et al., 2009b) materials based on the two-phase integro-differential model.

Furthermore, the integral nonlocal elasticity was reduced to differential nonlocal elasticity for certain special kernel functions by Eringen (1983). The differential nonlocal elasticity leads to a set of singular differential equations, and these equations could be simply solved; however, some difficulty exists when employing natural boundary conditions (Shaat, 2015). In the literature, the nonlocal differential model has been most widely used for bending, buckling and vibration analysis of nanorods, nanoplates and nanobeams (Guo and Yang, 2012; Duan and Wang, 2007; Lu et al., 2007; Aghababaei and Reddy, 2009; Thai et al. 2014). Also this nonlocal model is used for studying the vibration and buckling of functionally graded rectangular nano-plates based on nonlocal exponential shear deformation (Khorshidi et al. 2015; Khorshidi and Fallah, 2016). Some authors addressed the well-known paradoxical cantilever nonlocal beam problem (Challamel and Wang, 2008; Challamel et al., 2014; Wang et al., 2008), where an unreasonable stiffening effect was found in their results. Challamel and Wang (2008) also noted that this paradox can be solved with an integral-based model that combines the local and nonlocal curvatures in the constitutive relations. Most recently, Khodabakhshi and Reddy (2015) proposed a general finite-element formulation for the two-phase integro-differential nonlocal model to solve the well-known paradoxical cantilever nonlocal beam.

In all of the references outlined above, FEM-based approaches (i.e., classical and nonlocal-type FEM) have been used as the solution methods. Shaat (2015) stated that applying FE-based approaches to analyse nonlocal integral-type elastic problems required extremely challenging computational efforts. Furthermore, Khodabakhshi and Reddy (2015) noted that in the FE discretized integral model, due to the existence of the non-zero terms in the global stiffness matrix, the properties of the mesh distribution and also the need to increase the mesh size to achieve the desired accuracy, this approach demands a high computational cost.

The main contribution of this paper is the presentation of an efficient computational method to overcome these obstacles. To achieve this goal, the Ritz formulation based on the boundary characteristic orthogonal polynomials (BCOPs) for the two-phase integro-differential nonlocal elasticity model is presented. In addition, a novel set of BCOPs are derived based on the approach described by Bhat (2015) as trial functions in the Ritz method. These polynomials are generated using a modified Gram-Schmidt orthonormalization process. The advantage of the novel BCOPs is that not only the given geometrical boundary conditions are satisfied but also the natural boundary conditions. It should be noted that this method considerably improves the problem related to the bandwidth growth of the stiffness matrix in FEM-based approaches (Khodabakhshi and Reddy, 2015) because the orthogonality property of the BCOPs would lead to an increased number of zero entries in the stiffness matrix.

The nonlocal differential model has been used with the Rayleigh-Ritz method to calculate the natural frequencies of uniform and non-uniform nonlocal plates for several possible boundary conditions (Chakraverty and Behera, 2014; Behera and Chakraverty, 2016). Rayleigh-Ritz method has been used for local vibration analysis of moderately thick rectangular plates (Hashemi et al. 2009) and functionally graded rectangular plate (Khorshidi and Bakhsheshy, 2015). Faroughi and Goushegir (2016) studied the in-plane natural frequencies and mode shapes of non-uniform rectangular nanoplates using the Eringen nonlocal differential model along with the Rayleigh-Ritz method. Regarding the Eringen nonlocal differential model with the Rayleigh-Ritz method for modelling a nanoplate, to the best knowledge of the authors, the Ritz method using novel BCOPs has not been used to model two-phase integro-differential nonlocal elasticity. This efficient computational method is implemented here to study the static and dynamic analyses of two-phase integro-differential nonlocal plate problems. To date, this has not been carried out using any numerical

approaches. It is noteworthy that the method implemented here completely eliminates the challenges of generating elements within the influence zones (i.e., cohesive zones) in the NL-FEM.

The outline of the paper is as follows. Section 2 describes two-phase integro-differential nonlocal theory in 2D. The kernel function is expressed in section 3. Section 4 explains the Ritz method for nonlocal Kirchhoff plate theory. The construction of 2D novel BCOPs is explained in section 5. Numerical examples are given in section 6. Finally, some conclusions are drawn in section 7.

2. Two-phase integro-differential nonlocal theory in two dimensions

Eringen's nonlocal theory (Eringen, 1972) assumes that the stress at a reference point $\mathbf{x}$ in the body is dependent not only on the strain at $\mathbf{x}$ but also on the strain field at all other points ($\acute{\mathbf{x}}$) of the material. In the general integral-type nonlocal theory, this dependency is expressed as a weighted convolution integral in which the weighing function is a scalar kernel function $\mathrm{H}(\mathbf{x}, \acute{\mathbf{x}}, l_c)$. In Eringen's integral-type nonlocal theory, the stress at the point $\mathbf{x} \in \acute{\mathrm{V}}$ is given as

$$\boldsymbol{\sigma}(\mathbf{x}) = \int_{\acute{\mathrm{V}}} \mathrm{H}(\mathbf{x}, \acute{\mathbf{x}}, l_c)\mathbf{D} : \boldsymbol{\epsilon}(\acute{\mathbf{x}})\mathrm{d}\acute{\mathrm{V}} \tag{1}$$

where $\boldsymbol{\epsilon}(\acute{\mathbf{x}})$, $\mathbf{D}$ and $\acute{\mathrm{V}}$ denote the local strain at $\acute{\mathbf{x}}$, the fourth-order tensor of classical linear elastic-material moduli and the nonlocal continuum volume, respectively. The parameter l_c is the length-scale parameter.

According to Eringen (1987) and Altan (1989), both the local and nonlocal elastic models can be combined linearly and expressed as a more general two-phase nonlocal model. Equation (1) can be modified for a two-phase model to give

$$\boldsymbol{\sigma}(\mathbf{x}) = \eta_1\mathbf{D} : \boldsymbol{\epsilon}(\mathbf{x}) + \eta_2 \int_{\acute{\mathrm{V}}} \mathrm{H}(\mathbf{x}, \acute{\mathbf{x}}, l_c)\mathbf{D} : \boldsymbol{\epsilon}(\acute{\mathbf{x}})\mathrm{d}\acute{\mathrm{V}} \tag{2}$$

Where, volume fractions η_1 and η_2 denote local and nonlocal phases of the body material, respectively. The local η_1 and nonlocal-phase parameters η_2 are positive constants that should satisfy the following relation.

$$\eta_1 + \eta_2 = 1 \tag{3}$$

This model introduces two independent variables: the length scale, l_c, and local-phase parameter, η_1. However, the differential and integral forms of Eringen's model each considered only one length scale,l_c. l_c is the length scale parameter that depends on the internal characteristic length l_{in} by $l_c = e_0 l_{in}$, where, e_0 is a non-dimensional small length scale coefficient (lattice parameter, granular size or molecular diameters) and is appropriate with the description of the each nanostructure material that has to be calibrated with respect to dispersive wave properties of the Born-Kármán dynamics (Eringen, 1983), phonon dispersion curves (Ghosh et al. 2013), atomistic models or reliable experimental measurements.

3. Kernel function

The kernel function $\mathrm{H}(\mathbf{x}, \acute{\mathbf{x}}, l_c)$ imposes the shape of the nonlocal influence limited to a certain radial distance induced at $\mathbf{x}$ by the strain field at the points $\acute{\mathbf{x}}$ all over the body.

The kernel function $\mathrm{H}(\mathbf{x}, \acute{\mathbf{x}}, l_c)$ has the following features (Eringen, 1983):

* It is a positive function that has its maximum at the point $\mathbf{x} = \acute{\mathbf{x}}$ and is attenuated by increasing $\|\mathbf{x} - \acute{\mathbf{x}}\|$.
* It reverts to a delta function $\delta(\mathbf{x}, \acute{\mathbf{x}})$ as l_c approaches zero (i.e., when l_c is negligible, the constitutive equations simplify to the classical local equations.).

* It satisfies the normalization condition (where $\acute{V}$ is embedded in an indefinite domain $\acute{V}_\infty$):

$$\int_{\acute{V}_\infty} \mathrm{H}(\mathbf{x}, \acute{\mathbf{x}}, l_c)\mathrm{d}\acute{V} = 1 \tag{4}$$

* It is a bi-symmetric function:

$$\mathrm{H}(\mathbf{x}, \acute{\mathbf{x}}, l_c) = \mathrm{H}(\acute{\mathbf{x}}, \mathbf{x}, l_c) \tag{5}$$

* It approximates atomic lattice theory when l_c approaches the external characteristic length.

In the present study, the kernel function is chosen based on a modified non-singular stress-gradient kernel function proposed by Ghosh et al. (2014). The 2D stress-gradient kernel is defined as

$$\mathrm{H}(\gamma) = (2\pi l_c^2)^{-1} \exp(-\gamma)\,,\ \ \gamma = d/l_c\,,\ \ l_c = e_0 l_{in}\,,\ \ d = \|\mathbf{x} - \acute{\mathbf{x}}\|\,,\ \ \mathbf{x}, \acute{\mathbf{x}} \in \mathbb{R}^2 \tag{6}$$

where $d = \|\mathbf{x} - \acute{\mathbf{x}}\|$ represents the distance between two points in Euclidean space and l_{in} is the internal characteristic length (e.g., C-C bond spacing). The parameter e_0 is a material constant that is determined based on the acceptable accuracy of the nonlocal model relative to atomic-lattice theories or experiments. Fig. 1 shows the 2D kernel function of Eq. (6) for different cases of l_c, such as $l_c = 0.33$ nm, $l_c = 0.50$ nm and $l_c = 1.00$ nm. Fig. 1 shows that changing the length-scale parameter can alter the radius of the kernel-influence zone, while according to the condition of Eq. (4), the volume under the surface of the kernel remains constant. Subsequently, by increasing l_c, the kernel function can capture a broader range of interatomic interactions to give a stronger non-locality, close to those of the atomistic models. With decreasing l_c, the radius of influence becomes smaller and the kernel function approaches a Dirac delta function.

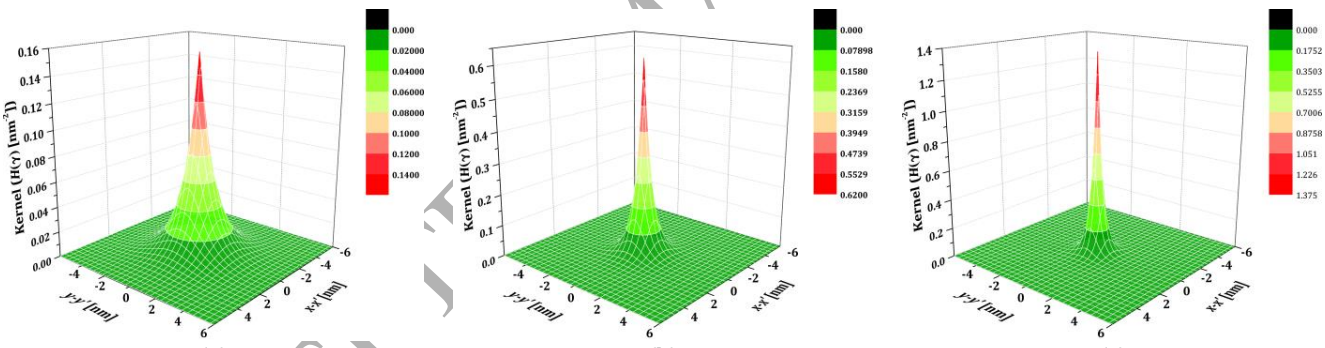

(a) (b) (c)

Fig. 1 Changes in the kernel function for different values of length-scale parameter: (a) $l_c = 0.33$ nm, (b) $l_c = 0.50$ nm and (c) $l_c = 1.00$ nm.

4. Ritz method for the nonlocal Kirchhoff plate theory

Consider a nanoscale thin rectangular elastic-plate model with length a, width b and height h, as shown in Fig. 2.

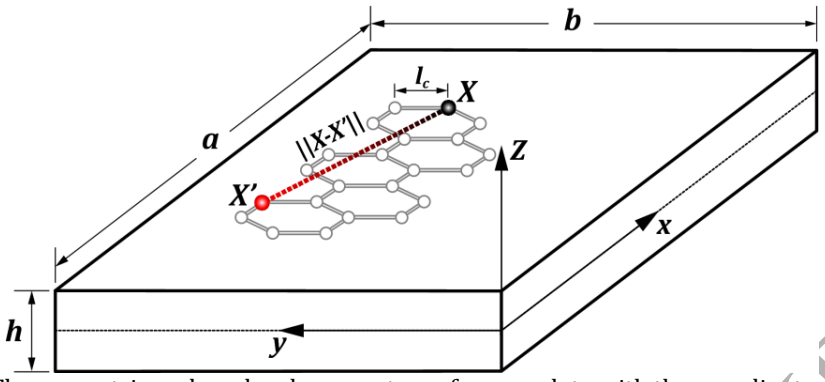

Fig. 2 The geometric and nonlocal parameters of a nanoplate with the coordinate system

The nonlocal strain energy of the nanoplate is given by:

$$\mathbb{U} = \frac{1}{2}\int_{\mathrm{V}} \boldsymbol{\epsilon} : \boldsymbol{\sigma}\, \mathrm{dV} \tag{7}$$

where, V is the volume of the nanoplate, $\boldsymbol{\epsilon}$ is the local strain tensor and $\boldsymbol{\sigma}$ is the nonlocal stress tensor at the point $\mathbf{x}$.

By substituting the nonlocal stress tensor $\boldsymbol{\sigma}$ from Eq. (2), the total two-phase nonlocal strain energy can be written as

$$\mathbb{U}\big(\boldsymbol{\epsilon}(\mathbf{x})\big) = \frac{1}{2}\int_{\mathrm{V}} \left(\eta_1 \boldsymbol{\epsilon}(\mathbf{x}) : \mathbf{D} : \boldsymbol{\epsilon}(\mathbf{x}) + \eta_2 \int_{\acute{\mathrm{V}}} \mathrm{H}(\mathbf{x}, \acute{\mathbf{x}}, l_c)\boldsymbol{\epsilon}(\mathbf{x}) : \mathbf{D} : \boldsymbol{\epsilon}(\acute{\mathbf{x}})\mathrm{d}\acute{\mathrm{V}}\right)\mathrm{dV} \tag{8}$$

The stain tensor in terms of out-of-plane displacement w_0 can be expressed as

$$\boldsymbol{\epsilon}(\mathbf{x}) = [\varepsilon_{xx} \quad \varepsilon_{yy} \quad \gamma_{xy}]^{\mathrm{T}}$$

where

$$\varepsilon_{xx} = -z\frac{\partial^2 w_0}{\partial x^2}\,,\quad \varepsilon_{yy} = -z\frac{\partial^2 w_0}{\partial y^2}\,,\quad \gamma_{xy} = -2z\frac{\partial^2 w_0}{\partial x \partial y}\,,\quad w_0 = w_0(x, y, t) \tag{9}$$

The elastic material moduli tensor for an isotropic case can be written as

$$\mathbf{D} = \begin{pmatrix} \mathcal{D}_{11} & \mathcal{D}_{12} & 0 \\ \mathcal{D}_{21} & \mathcal{D}_{22} & 0 \\ 0 & 0 & \mathcal{D}_{66} \end{pmatrix}$$

$$\mathcal{D}_{11} = \frac{E}{1-\nu^2}\,,\quad \mathcal{D}_{12} = \mathcal{D}_{21} = \frac{\nu E}{1-\nu^2}\,,\quad \mathcal{D}_{22} = \frac{E}{1-\nu^2}\,,\quad \mathcal{D}_{66} = G_{12} = \frac{E}{2(1+\nu)} \tag{10}$$

In which, E and ν are the Young's modulus and Poisson's ratio of the material, respectively, and G_{12} is the shear modulus.

Substituting Eqs. (9) and (10) into Eq. (8) and assuming the modal transverse displacement $w_0 = w(x, y)e^{i\omega t}$, the total potential and kinetic energies are

$$\mathbb{U}_{\boldsymbol{total}} = \frac{1}{2}\eta_1 \int_{\Omega}\left[\mathcal{Q}_{11}\left(\frac{\partial^2 w}{\partial x^2}\right)^2 + (\mathcal{Q}_{12}+\mathcal{Q}_{21})\frac{\partial^2 w}{\partial x^2}\frac{\partial^2 w}{\partial y^2} + \mathcal{Q}_{22}\left(\frac{\partial^2 w}{\partial y^2}\right)^2 + 4\mathcal{Q}_{66}\left(\frac{\partial^2 w}{\partial x \partial y}\right)^2\right] dxdy + \frac{1}{2}\eta_2 \int_{\Omega}\int_{\acute{\Omega}} \mathrm{H}(\boldsymbol{x},\acute{\boldsymbol{x}},l_c)\left[\mathcal{Q}_{11}\frac{\partial^2 w}{\partial x^2}\frac{\partial^2 w}{\partial \acute{x}^2} + \mathcal{Q}_{12}\frac{\partial^2 w}{\partial x^2}\frac{\partial^2 w}{\partial \acute{y}^2} + +\mathcal{Q}_{21}\frac{\partial^2 w}{\partial y^2}\frac{\partial^2 w}{\partial \acute{x}^2} + \mathcal{Q}_{22}\frac{\partial^2 w}{\partial y^2}\frac{\partial^2 w}{\partial \acute{y}^2} + 4\mathcal{Q}_{66}\frac{\partial^2 w}{\partial x \partial y}\frac{\partial^2 w}{\partial \acute{x}\partial \acute{y}}\right] d\acute{x}d\acute{y}\, dxdy + p\frac{1}{2}\int_0^b \left[M_{xx}^{nlocl} w + M_{xy}^{nlocl} w\right]_{x=0}^{x=a} dy + q\frac{1}{2}\int_0^a \left[M_{yy}^{nlocl} w + M_{xy}^{nlocl} w\right]_{y=0}^{y=b} dx + r\frac{1}{2}\int_0^b \left[M_{xx,x}^{nlocl} w + M_{xy,y}^{nlocl} w\right]_{x=0}^{x=a} dy + s\frac{1}{2}\int_0^a \left[M_{yy,y}^{nlocl} w + M_{xy,x}^{nlocl} w\right]_{y=0}^{y=b} dx \quad (11\text{-a})$$

$$\mathcal{Q}_{ij} = \frac{1}{12}\mathcal{D}_{ij}h^3\ ,\quad i,j = 1,2,6$$

$$\mathbf{T}_{\boldsymbol{total}} = \frac{1}{2}I_0\omega^2 \int_{\Omega} w^2 dxdy \quad (11\text{-b})$$

The parameters, p, q, r and s, control nonlocal boundary conditions at the four edges of the plate can be set to 0 and 1. For example, the SFSF boundary conditions require these parameters to be specified as: (p,q,r,s)=(1,1,0,1). The nonlocal bending (M_{xx}^{nlocl}) and twisting moments (M_{xy}^{nlocl}) are defined as

$$\begin{pmatrix} M_{xx}^{nlocl} \\ M_{yy}^{nlocl} \\ M_{xy}^{nlocl} \end{pmatrix} = -\begin{pmatrix} \mathcal{Q}_{11} & \mathcal{Q}_{12} & 0 \\ \mathcal{Q}_{21} & \mathcal{Q}_{22} & 0 \\ 0 & 0 & \mathcal{Q}_{66} \end{pmatrix} \int_{\acute{\Omega}} \mathrm{H}(x,y,\acute{x},\acute{y},l_c) \begin{pmatrix} \frac{\partial^2 w}{\partial \acute{x}^2} \\ \frac{\partial^2 w}{\partial \acute{y}^2} \\ 2\frac{\partial^2 w}{\partial \acute{x}\partial \acute{y}} \end{pmatrix} d\acute{x}d\acute{y} \quad (11\text{-c})$$

where, ω is the angular frequency, ρ is the mass per unit volume and $I_0 = \int_{-h/2}^{h/2} \rho dz = \rho h$ is the mass per unit area of the nanoplate.

The Ritz method has been applied to approximate the continuous model of the nanoplate by discretizing the displacement function $w(x,y)$ as a series in terms of admissible trial functions according to the following equation.

$$w(x,y) = \sum_{j=1}^{N} \mathbb{W}_j \widetilde{\Psi}_j(x,y) \quad (12)$$

In Eq. (12), the trial function $\widetilde{\Psi}_j$ forms a complete set of linearly independent admissible functions (Reddy, 2004) that satisfy at least the essential (or geometric) boundary conditions of the problem, and N denotes the order of approximation. The coefficients $\mathbb{W}_i$ are unknown constants that can be determined by minimizing the total energy function of the nonlocal plate model with respect to each unknown coefficient. The minimization of the total energy functional is equivalent to solving the following equation.

$$\frac{\partial(\mathbb{U}_{\boldsymbol{total}} - \mathbf{T}_{\boldsymbol{total}})}{\partial \mathbb{W}_r} = 0\ ,\quad r = 1,2,\dots,N \quad (13)$$

Which, results in the following generalized-eigenvalue problem regarding the free-vibration analysis of the nonlocal plate model.

$$([\mathbf{K}] - \omega^2[\mathbf{M}])\{\mathbf{W}\} = 0 \tag{14-a}$$

$$[\mathbf{K}] = \eta_1[\mathbf{K}]^{locl} + \eta_2[\mathbf{K}]^{nlocl} + [\mathbf{K}]^{pqrs} \tag{14-b}$$

where, $[\mathbf{K}]$ is the total stiffness matrix of the nanoplate, consisting of the local and nonlocal phases, $[\mathbf{K}]^{locl}$ and $[\mathbf{K}]^{nlocl}$, respectively. Also, $[\mathbf{K}]^{pqrs}$ is the stiffness matrix of nonlocal natural boundary conditions.

To study the static analysis of the two-phase integro-differential nonlocal plate model under various loadings, Eq. (15) can be used to obtain the static deflection function:

$$[\eta_1[\mathbf{K}]^{locl} + \eta_2[\mathbf{K}]^{nlocl} + [\mathbf{K}]^{pqrs}]\{\mathbf{W}\} = \{\mathbf{F}\} \tag{15}$$

where, $\{\mathbf{F}\}$ is the loading vector.

5. Construction of 2D novel BCOPs

In the Ritz method, the accuracy of the solution is highly dependent on the choice of the trial functions. Hence, to achieve reliable results, it is important to construct a suitable set of trial functions. In this paper, to this end, a new set of BCOPs has been derived as 2D trial functions. Following the development of Bhat (2015) for the 1D case, we derive novel BCOPs for the 2D case. The advantage of these polynomials is that they satisfy both the geometrical boundary conditions and the natural boundary conditions for local elasticity. However, these functions cannot satisfy the boundary conditions of a nonlocal plate having simply supported and free boundary conditions. This is due the fact that in nonlocal plate, the bending boundary condition is calculated as $M = \int_A z\left(\int_{\acute{V}} \mathrm{H}(\mathbf{x}, \acute{\mathbf{x}}, l_c)\mathbf{D} : \boldsymbol{\epsilon}(\acute{\mathbf{x}})\mathrm{d}\acute{V}\right)dA$ (Fernández et al., 2016).

The 2D trial function, $\widetilde{\Psi}_i$ can be separated in terms of 1D novel BCOPs in two orthogonal directions, ξ and η and the combination of $\mathbb{X}_p$ and $\mathbb{Y}_q$ is chosen from the first N terms of the following set.

$$\begin{gathered}\widetilde{\Psi}_i(\xi,\eta) = \{\mathbb{X}_1\mathbb{Y}_1, \mathbb{X}_2\mathbb{Y}_1, \mathbb{X}_1\mathbb{Y}_2, \mathbb{X}_3\mathbb{Y}_1, \mathbb{X}_2\mathbb{Y}_2, \mathbb{X}_1\mathbb{Y}_3, \mathbb{X}_p\mathbb{Y}_q, \dots, \mathbb{X}_{N-1}\mathbb{Y}_N, \mathbb{X}_N\mathbb{Y}_N\}, \\ p, q = 1,2,\dots,N \\ \xi = \frac{x}{a} \ , \quad \eta = \frac{y}{b}\end{gathered} \tag{16}$$

where, $\mathbb{X}_p : \xi \to \mathbb{X}_p(\xi)$ and $\mathbb{Y}_q : \eta \to \mathbb{Y}_q(\eta)$ are the new set of orthogonal polynomial functions generated in the ξ and η directions, respectively, using the modified Gram-Schmidt orthogonalization process. To construct the orthogonal polynomial set of functions $\mathbb{X}_p(\xi)$, the following procedure should be followed.

$$\begin{gathered}\mathbb{X}_1(\xi) = [h_0(\xi) - U_0]\mathbb{X}_0(\xi) \\ \mathbb{X}_{p+1}(\xi) = \left[h_p(\xi) - U_p\right]\mathbb{X}_p(\xi) - L_p\mathbb{X}_{p-1}(\xi)\end{gathered} \tag{17}$$

where,

$$h_p(\xi) = C_{1p}\xi + C_{2p}\xi^2 + C_{3p}\xi^3 + C_{4p}\xi^4 + \xi^5 \tag{18}$$

The function $h_p(\xi)$ is known as the "*evolution*" function. The constants $(C_{1p}, C_{2p}, C_{3p}, C_{4p})$ are obtained by satisfying the boundary conditions.

A complete set consisting of the linearly independent characteristic orthogonal polynomials produced by Eq. (17) will be formed and the orders of them steadily changes monotonically (Bhat, 2015).

The coefficients U_p and L_p can be derived from the following relations.

$$U_p = \frac{\int_0^1 \varrho(\xi) h_p(\xi) \mathbb{X}_p^2(\xi)\, d\xi}{\int_0^1 \mathbb{X}_p^2(\xi)\, d\xi}\ , \quad L_p = \frac{\int_0^1 \varrho(\xi) h_p(\xi) \mathbb{X}_p(\xi) \mathbb{X}_{p-1}(\xi)\, d\xi}{\int_0^1 \mathbb{X}_{p-1}^2(\xi)\, d\xi} \tag{19}$$

The novel BCOPs have the following orthogonality property.

$$\int_0^1 \varrho(\xi) \mathbb{X}_i(\xi) \mathbb{X}_j(\xi)\, d\xi = \begin{cases} 0 & i \neq j \\ \|\mathbb{X}_i(\xi)\| & i = j \end{cases} \tag{20-a}$$

$$\int_0^1 \varrho(\xi)\, d\xi > 0 \tag{20-b}$$

where, $\varrho(\xi)$ is a weight function. In the presence of variable thickness, variable density and young's modulus of the plate, the weight functions can be chosen as functions of spatial variables along two orthogonal directions (ξ, η) which will be dependent on which cases are imposed on the plate (Chakraverty, 2009). Here, for a uniform and homogeneous plate, $\varrho(\xi) = 1$. The coefficients of the evolution function and first terms of novel BCOPs are given in Table 1 for several boundary conditions in the ξ and η directions.

According to Bhat (2015), these new trial functions give an exact solution for problems in classical elasticity based on the Fourier-series expansion in terms of the novel BCOPs. Now, substituting Eq. (16) into Eq. (12) leads to a generalized-eigenvalue problem $([\mathbf{K}] - \omega^2[\mathbf{M}])\{\mathbf{W}\}=0$. The components of the stiffness and mass matrices are obtained as follows.

$$\mathbf{k}_{ij}^{locl} = \int_\Omega \left[\mathcal{Q}_{11} \frac{\partial^2 \widetilde{\Psi}_i(x,y)}{\partial x^2} \frac{\partial^2 \widetilde{\Psi}_j(x,y)}{\partial x^2} + \left(\mathcal{Q}_{12} + \mathcal{Q}_{21}\right) \frac{\partial^2 \widetilde{\Psi}_i(x,y)}{\partial x^2} \frac{\partial^2 \widetilde{\Psi}_j(x,y)}{\partial y^2} + \mathcal{Q}_{22} \frac{\partial^2 \widetilde{\Psi}_i(x,y)}{\partial y^2} \frac{\partial^2 \widetilde{\Psi}_j(x,y)}{\partial y^2} + 4\mathcal{Q}_{66} \frac{\partial^2 \widetilde{\Psi}_i(x,y)}{\partial x \partial y} \frac{\partial^2 \widetilde{\Psi}_j(x,y)}{\partial x \partial y} \right] dxdy$$

$$\mathbf{k}_{ij}^{nlocl} = \int_\Omega \int_{\hat{\Omega}} \mathrm{H}(\mathbf{x}, \acute{\mathbf{x}}, l_c) \left[\mathcal{Q}_{11} \frac{\partial^2 \Psi_i(x,y)}{\partial x^2} \frac{\partial^2 \Psi_j(\acute{x},\acute{y})}{\partial \acute{x}^2} + \mathcal{Q}_{12} \frac{\partial^2 \Psi_i(x,y)}{\partial x^2} \frac{\partial^2 \Psi_j(\acute{x},\acute{y})}{\partial \acute{y}^2} + \mathcal{Q}_{21} \frac{\partial^2 \Psi_i(x,y)}{\partial y^2} \frac{\partial^2 \Psi_j(\acute{x},\acute{y})}{\partial \acute{x}^2} + \mathcal{Q}_{22} \frac{\partial^2 \Psi_i(x,y)}{\partial y^2} \frac{\partial^2 \Psi_j(\acute{x},\acute{y})}{\partial \acute{y}^2} + 4\mathcal{Q}_{66} \frac{\partial^2 \Psi_i(x,y)}{\partial x \partial y} \frac{\partial^2 \Psi_j(\acute{x},\acute{y})}{\partial \acute{x} \partial \acute{y}} \right] d\acute{x} d\acute{y}\, dxdy \tag{21-a}$$

$$\mathbf{k}_{ij}^{pqrs} = pT_{ij}^x + pT_{ij}^y + rC_{ij}^x + sC_{ij}^y$$

$$\mathbf{m}_{ij} = I_0 \int_\Omega \widetilde{\Psi}_i(x,y) \widetilde{\Psi}_j(x,y) dxdy \tag{21-b}$$

where,

$$\begin{aligned}
T_{ij}^x &= \frac{1}{2} \int_0^b \left[\left(M_{xx}^{nlocl}\right)_i \widetilde{\Psi}_j(x,y) + \left(M_{xy}^{nlocl}\right)_i \widetilde{\Psi}_j(x,y) + \widetilde{\Psi}_i(x,y) \left(M_{xx}^{nlocl}\right)_j + \widetilde{\Psi}_i(x,y) \left(M_{xy}^{nlocl}\right)_j \right]_{x=0}^{x=a} dy \\
T_{ij}^y &= \frac{1}{2} \int_0^a \left[\left(M_{yy}^{nlocl}\right)_i \widetilde{\Psi}_j(x,y) + \left(M_{xy}^{nlocl}\right)_i \widetilde{\Psi}_j(x,y) + \widetilde{\Psi}_i(x,y) \left(M_{yy}^{nlocl}\right)_j + \widetilde{\Psi}_i(x,y) \left(M_{xy}^{nlocl}\right)_j \right]_{y=0}^{y=b} dx \\
C_{ij}^x &= \frac{1}{2} \int_0^b \left[\left(M_{xx,x}^{nlocl}\right)_i \widetilde{\Psi}_j(x,y) + \left(M_{xy,y}^{nlocl}\right)_i \widetilde{\Psi}_j(x,y) + \widetilde{\Psi}_i(x,y) \left(M_{xx,x}^{nlocl}\right)_j + \widetilde{\Psi}_i(x,y) \left(M_{xy,y}^{nlocl}\right)_j \right]_{x=0}^{x=a} dy \\
C_{ij}^y &= \frac{1}{2} \int_0^a \left[\left(M_{yy,y}^{nlocl}\right)_i \widetilde{\Psi}_j(x,y) + \left(M_{xy,x}^{nlocl}\right)_i \widetilde{\Psi}_j(x,y) + \widetilde{\Psi}_i(x,y) \left(M_{yy,y}^{nlocl}\right)_j + \widetilde{\Psi}_i(x,y) \left(M_{xy,x}^{nlocl}\right)_j \right]_{y=0}^{y=b} dx
\end{aligned} \tag{21-c}$$

In Eq. (21-a), the nonlocal trial functions can be defined as: $\widetilde{\Psi}_i(\acute{x},\acute{y}) := \widetilde{\Psi}_i(x,y)\big|_{\substack{x=\acute{x} \\ y=\acute{y}}}$.

The components T_{ij}^x, T_{ij}^y (C_{ij}^x, C_{ij}^y) are imposed to satisfy the bending moments at x=0 and x=a, y=0 and y=b, (shear transverse forces at x=0 and x=a, y=0 and y=b), respectively. And the nonlocal bending and twisting moments for the k-th member of the BCOP set can be rewritten as:

$$\begin{pmatrix}(M_{xx}^{nlocl})_k\\(M_{yy}^{nlocl})_k\\(M_{xy}^{nlocl})_k\end{pmatrix}=-\begin{pmatrix}Q_{11}&Q_{12}&0\\Q_{21}&Q_{22}&0\\0&0&Q_{66}\end{pmatrix}\int_{\Omega}H(x,y,\acute{x},\acute{y},l_c)\begin{pmatrix}\frac{\partial^2\widetilde{\Psi}_k(\acute{x},\acute{y})}{\partial\acute{x}^2}\\\frac{\partial^2\widetilde{\Psi}_k(\acute{x},\acute{y})}{\partial\acute{y}^2}\\2\frac{\partial^2\widetilde{\Psi}_k(\acute{x},\acute{y})}{\partial\acute{x}\partial\acute{y}}\end{pmatrix}d\acute{x}d\acute{y} \tag{22}$$

The vector of unknown coefficients in the Ritz-discretization series is given by

$$\{\mathbf{W}\}=[\mathbb{W}_1,\mathbb{W}_2,\dots,\mathbb{W}_N]^{\mathbf{T}} \tag{23}$$

Table 1. First terms and evolution functions of novel BCOPs for different boundary conditions of local plate

First term and evolution function	Boundary conditions in the ξ direction	
$\mathbb{X}_0(\xi)=\xi^2-2\xi^3+\xi^4$ $h_p(\xi)=-\frac{3}{2}\xi^2+\xi^3$	$\mathbb{X}_p(0)=\mathbb{X}'_p(0)=0$ $\mathbb{X}_p(1)=\mathbb{X}'_p(1)=0$ $h'_p(0)=0$ $h'_p(1)=0$	Clamped — Clamped
$\mathbb{X}_0(\xi)=\frac{3}{2}\xi^2-\frac{5}{2}\xi^3+\xi^4$ $h_p(\xi)=-\frac{3}{2}\xi^2+\xi^3$	$\mathbb{X}_p(0)=\mathbb{X}'_p(0)=0$ $\mathbb{X}_p(1)=\mathbb{X}''_p(1)=0$ $h'_p(0)=0$ $h'_p(1)=0$	Clamped — Simply Support
$\mathbb{X}_0(\xi)=\xi-2\xi^3+\xi^4$ $h_p(\xi)=-\frac{3}{2}\xi^2+\xi^3$	$\mathbb{X}_p(0)=\mathbb{X}''_p(0)=0$ $\mathbb{X}_p(1)=\mathbb{X}''_p(1)=0$ $h'_p(0)=0$ $h'_p(1)=0$	Simply Support — Simply Support
$\mathbb{X}_0(\xi)=6\xi^2-4\xi^3+\xi^4$ $h_p(\xi)=C_{2p}\xi^2+C_{3p}\xi^3+\xi^4$	$\mathbb{X}_p(0)=\mathbb{X}'_p(0)=0$ $\mathbb{X}''_p(1)=\mathbb{X}'''_p(1)=0$ $2h'_p(1)\mathbb{X}'_p(1)+h''_p(1)\mathbb{X}_p(1)=0$ $3h''_p(1)\mathbb{X}'_p(1)+h'''_p(1)\mathbb{X}_p(1)=0$	Clamped — Free
$\mathbb{X}_0(\xi)=1$ $h_p(\xi)=C_{1p}\xi+C_{2p}\xi^2+C_{3p}\xi^3+C_{4p}\xi^4+\xi^5$	$\mathbb{X}''_p(0)=\mathbb{X}'''_p(0)=0$ $\mathbb{X}''_p(1)=\mathbb{X}'''_p(1)=0$ $2h'_p(0)\mathbb{X}'_p(0)+h''_p(0)\mathbb{X}_p(0)=0$ $3h''_p(0)\mathbb{X}'_p(0)+h'''_p(0)\mathbb{X}_p(0)=0$ $2h'_p(1)\mathbb{X}'_p(1)+h''_p(1)\mathbb{X}_p(1)=0$ $3h''_p(1)\mathbb{X}'_p(1)+h'''_p(1)\mathbb{X}_p(1)=0$	Free — Free

In appendix A, the calculation of the coefficients C_i for two cases such as cantilever and free-free are presented.

6. Numerical Examples

In this section, the normalized deflection and non-dimensional natural frequencies of the two-phase integro-differential nonlocal Kirchhoff plate model can be obtained by employing Eqs. (14) and (15). The computed results are reported in the form of tables and graphs. To this end, a nonlocal uniform plate model with the following isotropic mechanical properties is considered as Table 2.

Table 2. Material properties of the considered nanoplate (Aghababaei and Reddy, 2009).

Young's Modulus	Poisson's Ratio	Mass per unit volume	Thickness
$E = 30 \times 10^6$ Pa	$\nu = 0.30$	$\rho = 100$ Kg/m^3	$h = 1$ nm

Furthermore, the effects of the local-phase parameter η_1, length-scale parameter l_c, and aspect ratio on the results are discussed for different boundary conditions. As illustrated in Fig. 3, the boundary conditions of the nanoplate are denoted by the letters C, S and F, which represent the clamped, simply supported and free cases, respectively, and begin with the edge condition at $x = 0$, counter clockwise.

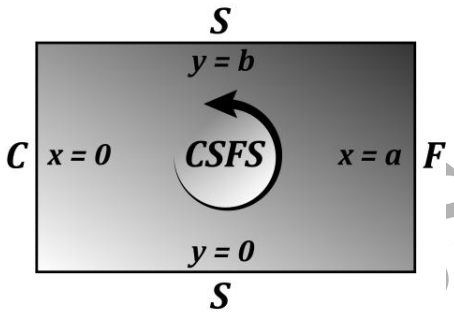

Fig. 3 Notation of the boundary conditions

In all case studies, the value of the aspect ratio a/b is assumed to be equal to 2, unless otherwise indicated. The integrals included in the stiffness matrix in Eq. (21-a) are calculated using a high-precision Cuhre cubature rule (Hahn, 2007). It should be noted that, to the best knowledge of the authors, there are no results for the static deflections and natural frequencies of the nanoplate modelled by the Eringen nonlocal integral model in the literature. Therefore, in Section 6.1, the Euler-Bernoulli beam has been studied to validate the findings of the proposed numerical approach through comparison with the available solution for nanobeams modelled by the two-phase integro-differential form of the Eringen nonlocal model. The reference results were obtained by Khodabakhashi and Reddy (2015). In Sections 6.2 and 6.3, the static deformation and natural frequencies of the nanoplate are studied. The numerical results achieved in both subsections demonstrate the abilities of the applied approach.

6.1. Validation

For validation, herein, we exploit an example that was studied by Khodabakhashi and Reddy (2015) using the two-phase integro-differential form of the Eringen nonlocal model. To this end, we consider a uniform clamped beam of length L, constant bending rigidity EI and uniformly distributed load intensity q_0. The maximum deflection associated with the local beam model is $W_l = \frac{q_0 L^4}{384EI}$, which occurs in the middle of the beam. The normalized maximum deflections, $\bar{W} = \frac{W_{nl}}{W_l}\Big|_{x=L/2}$, of a clamped beam are given in Table 3 for different values of local-phase parameter η_1 and l_c/L. W_{nl} and W_l are the nonlocal ($\eta_1 = 0$) and local maximum deflections of the beam, respectively.

Table 3. Normalized maximum deflections of clamped Euler-Bernoulli beam subjected to a uniformly distributed load

	Normalized deflection							
	$\eta_1 = 0$		$\eta_1 = 0.25$		$\eta_1 = 0.5$		$\eta_1 = 0.75$	
l_c/L	Present	Ref. (34)	Present	Ref. (34)	Present	Ref. (34)	Present	Ref. (34)

0.01	**1.0405**	**1.0307**	**1.0185**	**1.0151**	**1.0116**	**1.0074**	**1.0038**	**1.0029**
	$N=5$	$Nel=80$	$N=5$	$Nel=80$	$N=5$	$Nel=80$	$N=5$	$Nel=80$
	1.0436	**1.0387**	**1.0213**	**1.02**	**1.0126**	**1.0106**	**1.0052**	**1.0044**
	$N=6$	$Nel=90$	$N=6$	$Nel=90$	$N=6$	$Nel=90$	$N=6$	$Nel=90$
	1.0459	**1.0451**	**1.024**	**1.0239**	**1.0132**	**1.0131**	**1.0056**	**1.0056**
	$N=7$	$Nel=100$	$N=7$	$Nel=100$	$N=7$	$Nel=100$	$N=7$	$Nel=100$
0.015	**1.0975**	**1.0904**	**1.0512**	**1.0501**	**1.0282**	**1.0287**	**1.0126**	**1.0129**
	$N=8$	$Nel=80$	$N=8$	$Nel=80$	$N=8$	$Nel=80$	$N=8$	$Nel=80$
	1.099	**1.096**	**1.0534**	**1.0529**	**1.0302**	**1.0304**	**1.0139**	**1.0137**
	$N=9$	$Nel=90$	$N=9$	$Nel=90$	$N=9$	$Nel=90$	$N=9$	$Nel=90$
	1.1002	**1.1003**	**1.0549**	**1.0549**	**1.0317**	**1.0317**	**1.0143**	**1.0143**
	$N=10$	$Nel=100$	$N=10$	$Nel=100$	$N=10$	$Nel=100$	$N=10$	$Nel=100$
0.02	**1.1468**	**1.1421**	**1.0753**	**1.0776**	**1.0452**	**1.0449**	**1.0183**	**1.0203**
	$N=9$	$Nel=80$	$N=9$	$Nel=80$	$N=9$	$Nel=80$	$N=9$	$Nel=80$
	1.1481	**1.1466**	**1.0799**	**1.0794**	**1.0461**	**1.046**	**1.0199**	**1.0208**
	$N=10$	$Nel=90$	$N=10$	$Nel=90$	$N=10$	$Nel=90$	$N=10$	$Nel=90$
	1.15	**1.1495**	**1.0802**	**1.0802**	**1.0464**	**1.0464**	**1.0212**	**1.0211**
	$N=11$	$Nel=100$	$N=11$	$Nel=100$	$N=11$	$Nel=100$	$N=11$	$Nel=100$

The convergence of the present results for a clamped beam under a uniformly distributed load is demonstrated in the Fig. 4 for one case. In this case, the parameters l_c/L and η_1 are taken as 0.02 and 0.5, respectively.

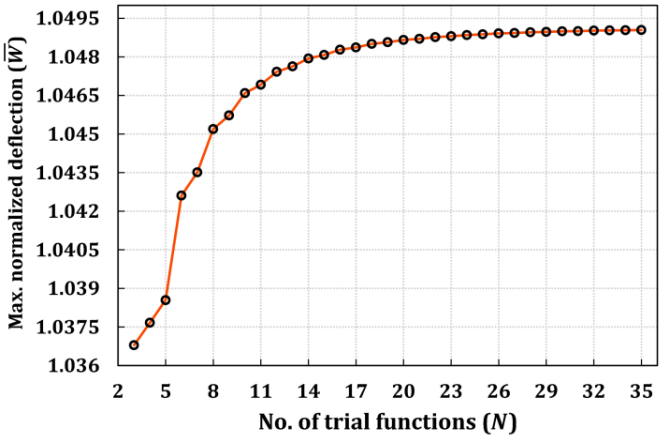

Fig. 4 Convergence of normalized maximum deflection of a clamped Euler-Bernoulli beam, under a uniformly distributed load for the case: $l_c/L = 0.02$ and $\eta_1 = 0.5$.

One can conclude from Table 3 that the results obtained by the new approach accurately converged to the results calculated by the NL-FEM. As seen, the proposed approach, NL-RM, significantly enhanced the convergence rate and reduced computational time compared to NL-FEM. According to the results reported in Table 3, the maximum order of approximation in NL-RM is 9, while to obtain the same results using NL-FEM, the mesh has 100 elements. Therefore, NL-FEM requires more memory than NL-RM. In addition, NL-RM does not need to determine which elements are within the influence zone, as with NL-FEM. Also, 2- and 3-dimensional problems are more challenging for NL-FEM (Khodabakhshi and Reddy, 2015).

6.2. Static analysis

In this section, numerical results are provided for the Kirchhoff plate theory with the Eringen two-phase integro-differential nonlocal model of the form of Eq. (15). As shown in Fig. 5, two different types of boundary conditions and loads are taken into account:

A. A uniformly distributed loaded plate with CFCF boundary conditions.
B. A plate with a concentrated load applied at the point (a, b) with CSFF boundary conditions.

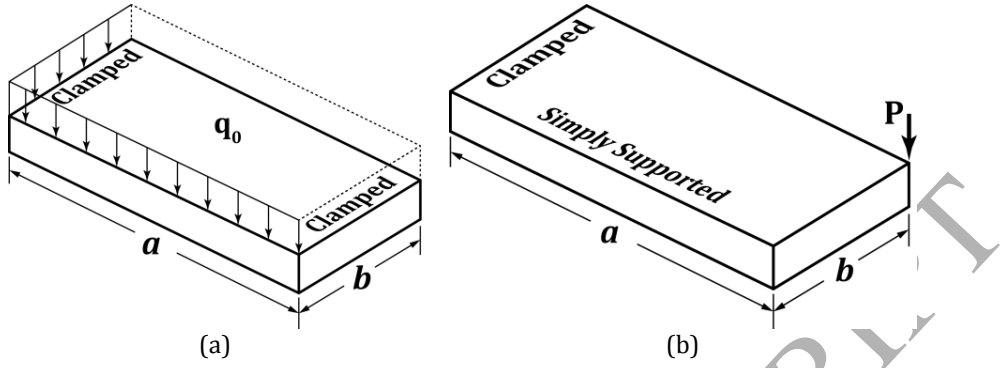

(a) (b)

Fig. 5. Two different cases of load and boundary conditions: (a) Case: A, (b) Case: B

To determine the necessary degree of the polynomial set, *N*, for acceptable results, a convergence study should be implemented. Studies of the convergence of the nonlocal deflection of the nanoplate for the CFCF and CSFF boundary conditions with an aspect ratio of 2 were performed. We concluded that the nonlocal deflection of the plate approaches the solutions when the total number of trial functions are *N*=10.

6.2.1 Case: A

The first case concerns an isotropic rectangular nanoplate, with length $a = 10$ nm and width $b = 5$ nm, subject to a uniformly distributed transverse load with intensity q_0. The material properties are given in Table 2. In this model, the deflection of the local Kirchhoff plate is obtained when the nonlocal-phase parameter η_2 and length-scale parameter l_c are considered to be zero. The maximum deflection of the conventional Kirchhoff plate is $\bar{w}(x, y)$ was obtained using the FEM solution. Then, the nonlocal deflections, $w(x, y)$, are normalized with respect to the maximum deflection of the local plate. Fig. 6 shows the nonlocal deflections of the plate for 3 different values of the length-scale parameter, $l_c =$ 0.5nm, 0.75nm and 1nm, as well as for local deflections of the plate, $l_c =$ 0nm. The results are obtained by taking into account only the first ten terms of the discretized series ($N = 10$) in the Ritz technique. As shown in Fig. 6, increasing the length-scale parameter causes the nanoplate to become more flexible and, as a result, the deflection of the plate is increased. It is clear that the normalized maximum deflection of the nanoplate is increased to 1.25, 1.41 and 1.60 for different values of $l_c =$ 0.5nm, 0.75nm and 1nm, respectively.

Next we explore the influence of the local-phase parameter, η_1, on the maximum normalized deflection of the nanoplate. Here, we considered different values for the local-phase parameter. Fig. 7 shows the results for the maximum normalized deflection for various values of the local-phase parameter and three different length scales. One can conclude from Fig. 7 that when the length scale is fixed, the maximum normalized deflection decreases with the increasing local-phase parameter. For example, for a length-scale value of 0.75nm and a range of 0–1 for the local-phase parameter, the maximum normalized deflection falls into the range of 1.51-1. However, increasing the length scale with a constant local-phase parameter, the maximum normalized deflection increases. Thus, the nanoplate becomes more flexible when the length parameter increases and the local-phase parameter decreases. Both of these changes cause a nonlocal effect, more than a local effect, in the nanoplate.

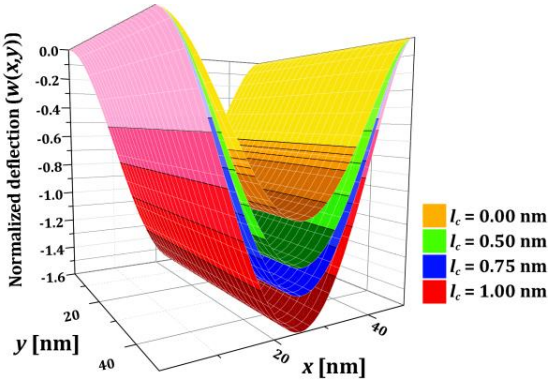

Fig. 6 Deflection shape of the CFCF nanoplate subjected to a uniformly distributed load for different values of the length-scale parameter

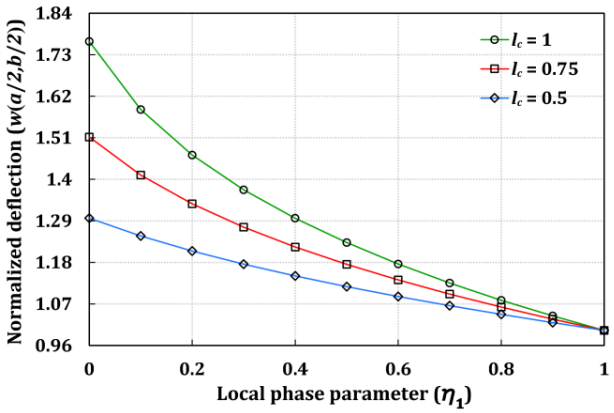

Fig. 7. Variation of the maximum normalized deflection of the nanoplate for different values of the local-phase parameter and length scale

6.2.2 Case: B

Another example considers the static deflection of a nanoplate subjected to a concentrated load with CSFF boundary conditions. The material parameters are given in Table 2. The maximum conventional deflection of this plate, which can be obtained using FEM at the free corner, is $\bar{w}(x, y)$. It should be noted that the corresponding force vector $\{\mathbf{F}\}$ in Eq. (15) is as follows.

$$\{\mathbf{F}\} = P\{\Psi_1, \Psi_2, \dots, \Psi_N\}^{\mathbf{T}}\Big|_{\substack{x=a \\ y=b}} \tag{24}$$

The nonlocal deflection of the plate is normalized with respect to the local maximum deflection. These nonlocal deflections are achieved by considering the first ten novel orthogonal polynomials ($N = 10$). Fig. 8 shows the results associated with $\eta_1 = 0$ and different values of the length-scale parameters. According to Fig. 8, as anticipated, the deflection of the plate increases when the length-scale parameter increases. This is because increasing the length scale causes the plate to soften and hence deflections are increased. In this case, the increase in deflection is not very large. For example, the maximum increase in the deflection of the plate is 27.5% for $l_c = 1$nm.

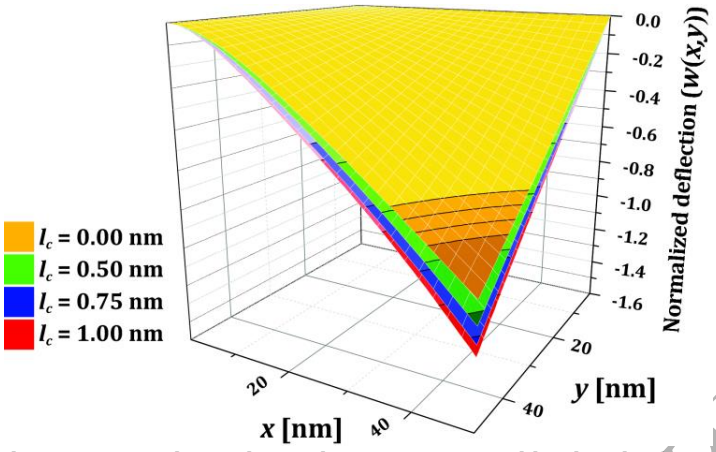

Fig. 8. Deflection shape of the CSFF nanoplate subjected to a concentrated load at the free corner of the nanoplate for different values of the length-scale parameter.

Fig. 9 shows the influence of the local-phase parameter η_1 on the normalized maximum deflection of the plate with CSFF boundary conditions. The results are presented for three different values of the length-scale parameter and the variation of the local-phase parameter from zero to one. As shown in Fig. 9, when l_c is fixed, the maximum normalized deflection decreases with increasing η_1. For example, for a length-scale value 0.75nm and a range of 0–1 for the local-phase parameter, the maximum normalized deflection lies in the range 1.2-1. According to Fig. 9, the maximum normalized deflection increases when the local-phase parameter decreases and the length scale parameter increases. Similar to case A, the results demonstrate that the deflection decreases with the increase in the local-phase parameter. This is because the nonlocal counterpart is gradually removed in Eq. (15) when the local-phase parameter gradually increases from 0 to 1.

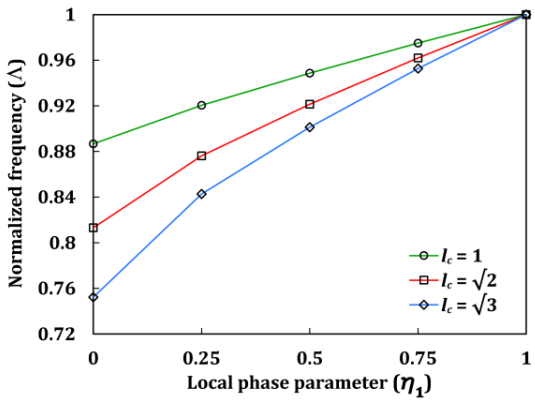

Fig. 9. Variation of the maximum normalized deflection of a cantilever nanoplate with η_1 for different values of l_c.

It is worth mentioning that both parameters l_c and η_1 impact the deflections of the nanoplate. The change of the length-scale parameter directly affects the shape of the nonlocal-distribution effect in the kernel function H(γ), which determines the long-range interatomic interactions in the nanostructures, whereas changes in the local-phase parameter directly affect the distributions of the local and nonlocal portions of the elastic-material model over the constitutive equations of motion.

6.3. Dynamic analysis

In this section, the free vibration of rectangular Kirchhoff nanoplates is studied based on two-phase integral-type nonlocal theory. To this end, the generalized-eigenvalue problem in Eq. (14) is numerically solved using the Ritz method with the novel BCOPs as the basis functions. The mechanical properties of the plate are given in Table 2. Here, the effects of three parameters, l_c, η_1, and the aspect ratio, on the frequencies are studied for various boundary conditions. We consider a nanoplate with two different boundary conditions, SSSS and CFFF. Similar to the static analysis, there are no published results of dynamic analysis of the Kirchhoff nanoplate based on the two-phase integral-differential Eringen model. The non-dimensional frequencies according to the local plate model are $\bar{\omega}_{locl} = \omega a^2\sqrt{I_0/\mathcal{D}_{11}}$. However, the non-dimensional frequencies according to the nonlocal plate model, $\bar{\omega}_{nlocl}$ are obtained by considering $\eta_1 = 0$ and $\eta_2 = 1$.

6.3.1 Effect of the local-phase parameter

First, we investigated the effect of the local-phase parameter η_1 on the normalized natural frequencies, Λ, which are calculated by dividing the non-dimensional nonlocal frequencies by the non-dimensional local frequencies ($\Lambda = \bar{\omega}_{nlocl}/\bar{\omega}_{locl}$). The first three non-dimensional frequencies of the local plate with SSSS and CFFF boundary conditions are given in Table 4. It should be noted that the aspect ratio of the plate is 2.

Table 4. The first three non-dimensional frequencies of the plate with an aspect ratio 2 and two different boundary conditions, SSSS and CFFF

Boundary conditions	Mode 1	Mode 2	Mode3
SSSS	49.34803	78.95685	128.3049
CFFF	3.516015	14.84119	22.03449

Fig. 10 shows the normalized natural frequencies for three different values of the length-scale parameter: $l_c =$ 1nm, 2nm and 3nm. One can conclude from Fig. 10 that for the purely nonlocal case ($\eta_1 = 0$), an increase in l_c causes the plate to become softer and consequently the natural frequencies of the plate decrease. This is consistent with most of the results reported in the literature concerning the differential Eringen nonlocal model (for example, Chakraverty and Behera 2014, Faroughi and Goushegir, 2016). It is observed from Fig. 10 that for a constant value of l_c, the normalized natural frequencies decrease with the decreasing local-phase parameter η_1, which represents an increase in the nonlocal contribution in Eq. (14). According to Fig. 10, the normalized frequency is decreased more in the higher modes of vibration than in the lower modes, for constant values of l_c and η_1. This is because in the higher modes, the wavelengths become shorter and hence the long-range interatomic interactions of the atoms increase, which increases the nonlocal effect.

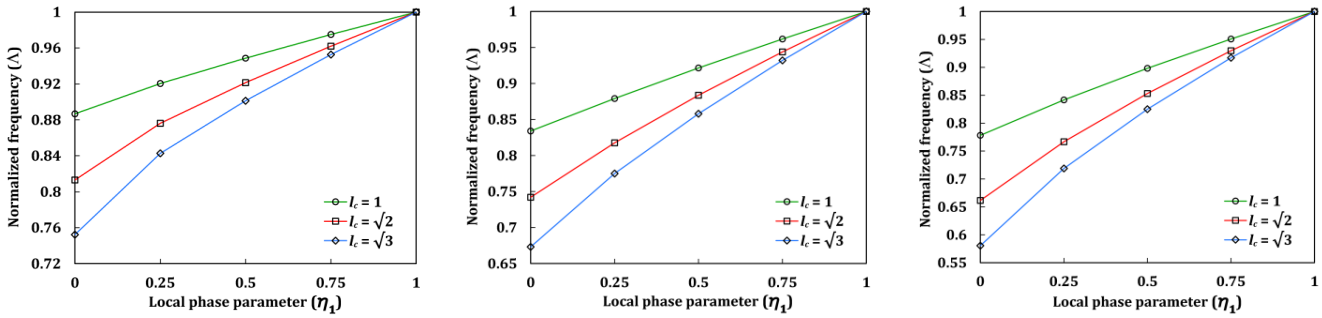

(a) (b) (c)

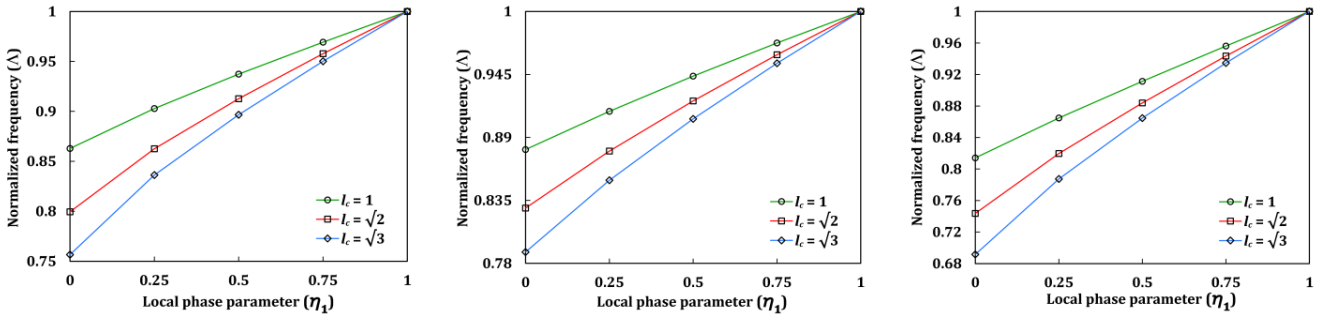

(d) (e) (f)

Fig. 10 Variation of the normalized frequencies of nanoplates with η_1 for different values of l_c with considering boundary conditions of: (a) SSSS (Mode 1) , (b) SSSS (Mode 2), (c) SSSS (Mode 3), (d) CFFF (Mode 1), (e) CFFF (Mode 2) and (f) CFFF (Mode 3).

6.3.2 Effect of the length scale parameter

Next, the effect of the length-scale parameter l_c on the first three non-dimensional natural frequencies of the plate is presented. Here, the material, geometrical and boundary conditions are similar to those in the first case. Fig. 11 shows the first three natural frequencies of the plate for six different values of l_c. In this example, the first three frequencies of the plate are obtained by two different nonlocal theories: the Eringen purely nonlocal integral- and differential-form models. The results using the Eringen differential model were obtained by Chakraverty and Behera (2014). As shown in Fig. 11, the natural frequencies decrease with the increasing length-scale parameter for both nonlocal theories. This is due to fact that an increase in l_c causes the plate to soften and therefore decreases the natural frequencies of the plate. According to Fig. 11, the natural frequencies of the plate obtained by the integral-type nonlocal model drop more sharply than those of the differential-type solution. This disparity arises due to the use of different kernel functions in this study and in the differential Eringen nonlocal model used by Chakraverty and Behera (2014). Here, the kernel function presented by Ghosh et al. (2014) was used. The advantage of this kernel function is that it provides the largest radius of influence and accounts for the longer-range interactions seen in the molecular model (Ghosh et al., 2014).

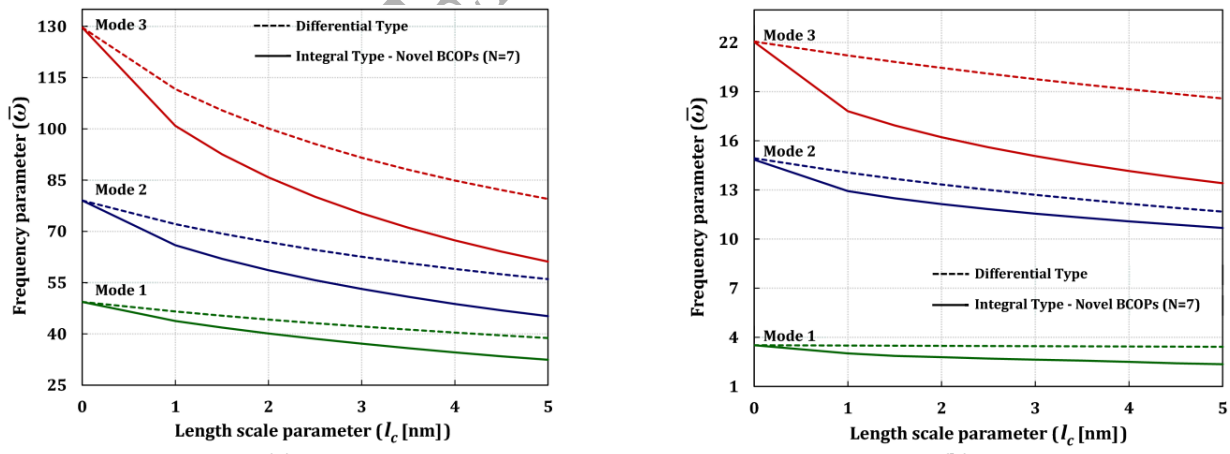

(a) (b)

Fig. 11 Variation of the first three frequency parameters of the nanoplates with l_c and a comparison of the two differential- and integral-type nonlocal plate models: (a) SSSS and (b) CFFF.

6.3.3 Effect of the aspect ratio

Finally, the effect of the aspect ratio on the normalized fundamental natural frequency is studied. The mechanical properties of the plate are given in Table 2. SSSS and CFFF are considered to be the boundary conditions of the plate and the width of plate is taken as $b = 10$ nm. Fig. 12 shows the normalized fundamental natural frequency of the plate for different values of the aspect ratio and the length-scale parameter. According to Fig. 12, the normalized frequency of the plate increases with increasing aspect ratio. It is clear that an increase in the aspect ratio is equivalent to an increase in the length of the plate, which makes the plate stiffer and consequently increases the frequency of the plate. In the literature, similar behaviour has been reported based on the differential-type nonlocal plate theories (e.g., Chakraverty and Behera, 2014; Ke et al., 2014 and Murmu and Pradhan, 2009).

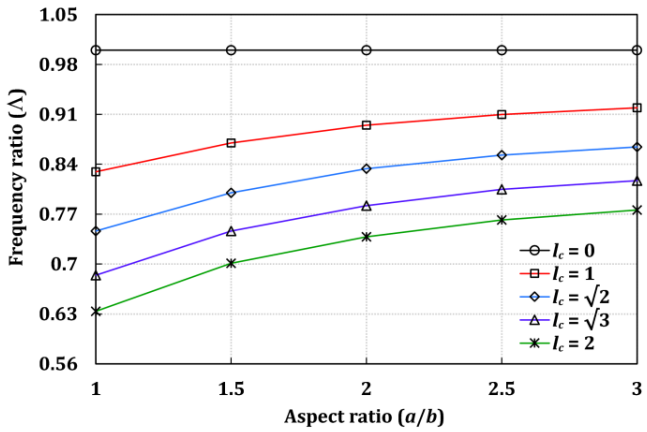

Fig. 12 Variation of the fundamental frequency ratio of an SSSS nanoplate with aspect ratios for different values of l_c.

6.4. A brief comment on the solution model

The aim of this section is to provide a short explanation about the efficiency of the proposed solution method. As previously mentioned, the procedure of the NL-FEM is associated with some limitations and challenges in solving 2D problems based on the integral form of the nonlocal elasticity theory. In the NL-FEM procedure, the nonlocal stiffness matrix relies on the mesh distribution. It converges to reliable results by increasing the number of elements. This increase in the number of elements increases the number of off-diagonal non-zero entries of the global stiffness matrix, resulting in a greatly increased number of calculations and high memory requirements (Khodabakhashi and Reddy, 2015). The proposed method completely overcomes the dependency of the solution on the mesh conditions. The reasons for the superiority of this method are summarized below.

1) **An efficient mesh-free approach:** *Due to the fact that, unlike the mesh-based analysis, the Ritz method is only based on the concept of increasing the DOFs and does not require mesh generation. The application of the Ritz method in the integral-type nonlocal elastic models can be very effective, especially for the 2D and 3D problems in which the selection of the elements within the influence zones and near the boundaries of the spatial domain is difficult and complicated.*
2) **Fast convergence:** *As demonstrated before, using the novel BCOPs as the basis functions increases the convergence rate of the Ritz solution very significantly. Khodabakhshi and Reddy (2015) showed that in the NL-FEM, the results of the 1D Euler-Bernoulli beam-bending problem are highly sensitive to the mesh size and hence a large number of elements were used in their analysis (i.e., $N_{el} = 100$). In the case of 2D and 3D problems, as expected, many more elements must be taken into account, which is computationally very expensive, whereas the results of the current method indicated that by considering only a few terms of the novel BCOPs, the solution of the Ritz approach converges to an accurate result rapidly. This feature can be particularly useful for higher modes of vibration.*
3) **Reduction of non-zero entries:** *The issue of increasing the number of non-zero entries and the bandwidth expansion of the nonlocal stiffness matrix in the NL-FEM has been resolved by the use of novel BCOPs due to the*

orthogonality property of Eq. 20. The orthogonality property of the BCOPs restricts the values of some off-diagonal entries of the stiffness matrix to zero.

To better understand this issue, Fig. 13 shows the structure of the symmetric total stiffness matrix $[\boldsymbol{K}]$ *of a fully-simply supported (SSSS) square nanoplate. The local-phase parameter is fixed* ($\eta_1 = 0.5$)*, along with the length scale parameter* $l_c = 2nm$*. The stiffness matrix is computed using the Ritz method by taking into account 20 terms of novel BCOPs in the discretized series. It can be shown that approximately* 72% *of the entries in the stiffness matrix are zero due to the orthogonality property of the novel BCOPs.*

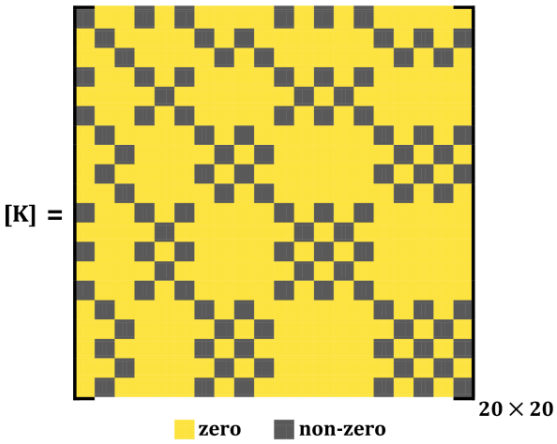

Fig. 13 Total stiffness-matrix structure of a two-phase CCCC square nanoplate with $\eta_1 = 0.5$ and $N = 20$.

4) **Super-fast runtime:** The *implementation of the proposed method was highly satisfactory and the computations were executed quickly in the short timeframes. In this regard, a comparison study should be carried out to better understand the computational efficiency of the proposed method. To this end, the SSSS nanoplate considered in the previous item is again considered in this subsection. The variation of the runtime (min) is plotted against the order of approximation (N), which is shown in Fig. 14. The executions are carried out on a 2.6GHz Intel(R) Core(TM) i7-4510U CPU with 8192MB memory for the three types of basis functions, namely, sinusoidal, orthogonal polynomials, satisfying only the geometrical boundary condition, and novel BCOPs. According to Fig. 14, for* $N = 13$*, the runtimes for the sinusoidal basis functions and the old BCOPs reach* $342.8\,min$ *and* $85.4\,min$*, respectively, while for the novel BCOPs, the solution is obtained much faster (6.65 min). Applying the novel BCOPs in the Ritz method remarkably enhances the computing speed, saves a great deal of CPU and RAM memory usage and simultaneously gives more accurate results. Therefore, the proposed method is a promising approach for dealing with two- and three-dimensional integral-type nonlocal problems with ease and without great computational effort.*

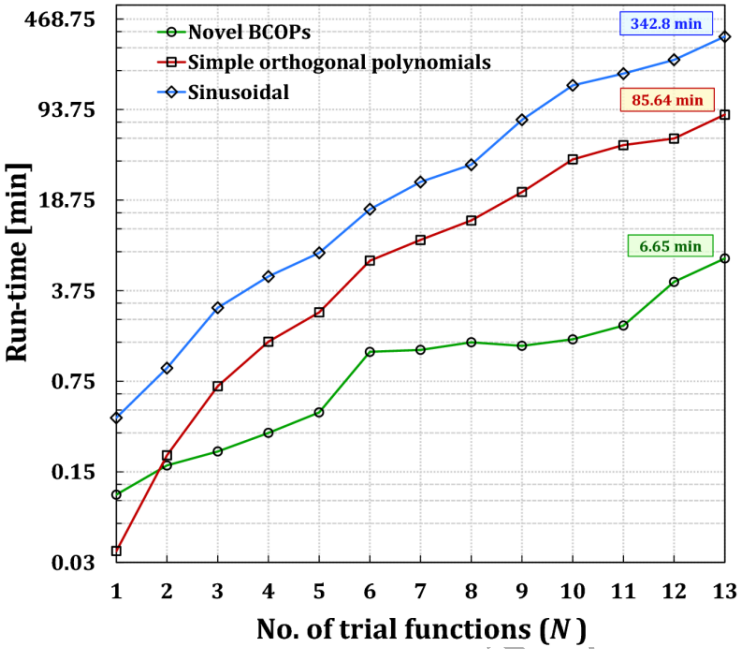

Fig. 14 Increasing the computation-execution time by increasing N for different types of basis functions, as applied using the Ritz method.

6.5. The orthogonality effects of derivatives of BCOPs

Herein, we intend to provide some numerical results to show the orthogonality effects of second-order derivatives of BCOPs on the entries of local and nonlocal stiffness and matrices. In this numerical example, the plate is considered fully simply-supported, the length scale parameter is equal to 3nm and the integration domain in x and y directions is 0.20nm and 0.15nm respectively. Also, the total number of trial functions are taken as N=9. The following notation is used here denoting the multiplicative terms of stiffness:

$$T_{pqrs} = \int_{\Omega} \left(\frac{\partial^{p+q} \widetilde{\Psi}_i(x,y)}{\partial x^p dy^q} \frac{\partial^{r+s} \widetilde{\Psi}_j(x,y)}{\partial x^r dy^s} \right) dxdy \tag{25}$$

$$\acute{T}_{pqrs} = \int_{\Omega} \int_{\acute{\Omega}} \mathrm{H}(x,y,\acute{x},\acute{y},l_c) \left(\frac{\partial^{p+q} \widetilde{\Psi}_i(x,y)}{\partial x^p dy^q} \frac{\partial^{r+s} \widetilde{\Psi}_j(\acute{x},\acute{y})}{\partial \acute{x}^r d\acute{y}^s} \right) d\acute{x}d\acute{y}\, dxdy$$

$$\Omega = \acute{\Omega} = \langle 0 \dots 20, 0 \dots 15 \rangle$$

where,

$$\Omega = \acute{\Omega} = \langle 0 \dots 20, 0 \dots 15 \rangle$$

and $\mathrm{H}(x,y,\acute{x},\acute{y},l_c)$ is the kernel function. Using the stiffness and mass relations given by Eq. (21), the multiplicative terms of trial functions are calculated and presented in Table 5. The orthogonality effect of these terms on the stiffness and mass matrices is investigated.

Table 5: The multiplicative terms of 2D BCOP trial functions in the components of stiffness and mass matrices obtained by the present nonlocal plate model

Multiplicative terms			
Order of derivatives	Local stiffness ($\boldsymbol{k}_{ij}^{locl}$)	Nonlocal stiffness ($\boldsymbol{k}_{ij}^{nlocl}$)	Mass ($\boldsymbol{m}_{ij}$)
$\mathbf{D}xx, \mathbf{D}xx$	T_{2020}	$\acute{T}_{2020}$	-

$\mathbf{D}xy, \mathbf{D}xy$	T_{1111}	$\acute{T}_{1111}$	-
$\mathbf{D}yy, \mathbf{D}yy$	T_{0202}	$\acute{T}_{0202}$	-
No derivatives	-	-	T_{0000}

Based on numerical analysis of Eq. (24), the percentage of zero terms exists in the second-order multiplicative terms for both local and nonlocal stiffness matrices for three different cases are as follows.

Case 1: The percentage of zero terms in the local and nonlocal entries of stiffness matrix (T_{2020} and $\acute{T}_{2020}$) is 81% and 72% respectively.

Case 2: The percentage of zero terms in the local and nonlocal entries of stiffness matrix (T_{1111} and $\acute{T}_{1111}$) is 72%.

Case 3: The percentage of zero terms in the local and nonlocal entries of stiffness matrix (T_{0202} and $\acute{T}_{0202}$) is 84% and 72% respectively. .

Case 4: Finally, for the mass term T_{0000}, the BCOP trial functions is perfectly orthogonal and only the diagonal terms are non-zero. This confirms the existence of orthogonal property in BCOPs. Obviously, in this case the percentage of non-zero values have the highest portions (89%) among the other cases of interest.

Although the second derivatives of trial functions are considered, all the local terms in cases 1 to 3, have shown many zero values in the present numerical example, ranging from 72% to 84% which significantly enhances the computational performance by processor especially for nonlocal terms. One may conclude that all the nonlocal terms certainly retain their ratios of non-zero to zero values, i.e. 28% to 72%. This agrees with the structure of stiffness matrix, shown in Fig. (13). As indicated in section 6.4, the BCOPs keep this ratio constant for the two-phase nonlocal stiffness matrix even with increasing N, unlike the NL-FEM/FEM that have the ill-conditioned problem of increasing bandwidth (Khodabakhshi and Reddy, 2015).

7. Conclusions

This study presented an efficient computational approach for solving boundary-value problems of nonlocal engineering interest. This technique uses the Ritz method, based on novel BCOPs, for implementation in a nonlocal context, which is known as NL-RM. The novel BCOPs are generated based on a modified Gram-Schmidt method and satisfy geometrical boundary conditions as well as natural boundary conditions. The goal of this approach is to resolve the obstacles in using a conventional numerical approach, such as NL-FEM. Here, a two-phase integro-differential nonlocal model is considered; thus, the constitutive equation of the system is a linear combination of local and nonlocal phase theories. This nonlocal model has two independent variables: the local-phase parameter η_1 and length scale parameter l_c. The NL-RM formulation for the two-phase integro-differential nonlocal model is introduced, and demonstrated here on a Kirchhoff plate. A modified two-dimensional stress-gradient kernel function is used as the attenuating function in the proposed nonlocal model, which is different from the kernel function related to Eringen's differential nonlocal theory. The method is verified using the results available in the literature for the one-dimensional case of the nonlocal Euler-Bernoulli beam model and good agreement is found. The results show the capability and superiority of the method with respect to NL-FEM. The effects of the length-scale parameter and local-phase parameter on the normalized deflection of the nanoplate are studied under two different loadings and boundary conditions. In addition to the two variable parameters, the effect of the aspect ratio on the natural frequencies is investigated in several numerical examples. The results show that decreasing the local-phase parameter and increasing the length-scale parameter make the plate more flexible and consequently increase the static deflections and decrease the natural frequencies of the plate.

As shown in this paper, the proposed method can be used as a highly effective and easy-to-handle numerical tool for analysing integral-type nonlocal problems. This approach greatly alleviates the inconvenience and challenges of numerical implementation stemming from mesh-based methods, such as NL-FEM. It is realized that, compared with other prevalent functions, the novel BCOPs are the best possible basis functions in the Ritz method to analyse problems

based on the integral form of the nonlocal elasticity theory. The strategy presented in this study can be applied as a powerful and straightforward approach for static and dynamic analyses of other beam, plate and shell theories, which suggests directions for future studies.

References

Aghababaei, R., Reddy, J.N., 2009, Nonlocal third-order shear deformation plate theory with application to bending and vibration of plates. *Journal of Sound and Vibration.* 326 (1-2): 277-289.

Altan, S.B., 1989, Existence in nonlocal elasticity. *Archive Mechanics* 41, 25–36.

Bazant, Z, Cedolin, L., 2010, *Stability of Structures: Elastic, Inelastic, Fracture and Damage Theories*, 3rd edition, World Scientific Publishing.

Behera, L., Chakraverty, S., 2016, Effect of scaling effect parameters on the vibration characteristics of nanoplates. *Journal of Vibration and Control.* 22 (10): 2389-2399.

Benvenuti, E. and Simone, A., 2013. One-dimensional nonlocal and gradient elasticity: closed-form solution and size effect. *Mechanics Research Communications*, *48*, pp.46-51.

Bhat, R.B., 2015, Vibration of beams using novel boundary characteristic orthogonal polynomials satisfying all boundary conditions. *Advances in Mechanical Engineering.* 7 (4).

Chakraverty, S., Behera, L., 2014, Free vibration of rectangular nanoplates using Rayleigh–Ritz method, *Physica E: Low-dimensional Systems and Nanostructures*, Volume 56, February 2014, Pages 357-363.

Challamel, N., Wang, C.M., 2008, The small length scale effect for a non-local cantilever beam: A paradox solved. *Nanotechnology*, 19(34), 345703(7).

Challamel, N., Zhang, Z., Wang, C.M., Reddy, J.N., Wang, Q., Michelitsch, T., Collet, B., 2014, On nonconservativeness of Eringen's nonlocal elasticity in beam mechanics: Correction from a discrete-based approach. *Archive of Applied Mechanics*, 84(9–11), 1275–1292.

Duan, W.H., Wang, C.M., 2007, Exact solutions for axisymmetric bending of micro/nanoscale circular plates based on nonlocal plate theory. *Nanotechnology*. 18 (38).

Edelen, D.G.B., Green, A.E., Laws, N., 1971, Nonlocal continuum mechanics. *Archive for Rationale Mechanics and Analysis* 43, 36–44.

Edelen, D.G.B., Laws, N., 1971, On the thermodynamics of systems with nonlocality. *Archive for Rationale Mechanics and Analysis* 43, 24–35

Eringen, A.C., 1972, Nonlocal polar elastic continua. *International Journal of Engineering Science*, 10(1), 1–16.

Eringen, A.C., 1983. On differential equations of nonlocal elasticity and solutions of screw dislocation and surface waves. *J. Appl. Phys.* 54 (9), 4703–4710.

Eringen, A.C., 1987, Theory of nonlocal elasticity and some applications. *Res Mechanica* 21, 313–342.

Eringen, A.C., Edelen, D.G.B., 1972, On nonlocal elasticity. *International Journal of Engineering Science* 10, 233–248.

Faroughi, S., Goushegir, S.M.H., 2016, Free in-plane vibration of heterogeneous nanoplates using Ritz method". *Journal of Theoretical and Applied Vibration and Acoustics*, 2(1), Pages 1-20, ISSN 2423-4761.

Fernández-Sáez, J., Zaera, R., Loya, J.A. and Reddy, J.N., 2016. Bending of Euler–Bernoulli beams using Eringen's integral formulation: a paradox resolved. *International Journal of Engineering Science*, *99*, .107-116.

Ghosh, S., Sundararaghavan, V., Waas, A.M., 2014, Construction of multi-dimensional isotropic kernels for nonlocal elasticity based on phonon dispersion data. *International Journal of Solids and Structures*. 51 (2): 392-401.

Ghosh, S., Kumar, A., Sundararaghavan, V. and Waas, A.M., 2013, Non-local modeling of epoxy using an atomistically-informed kernel. International Journal of Solids and Structures, 50(19), 2837-2845

Guo, S.Q. and Yang, S.P., 2012. Axial vibration analysis of nanocones based on nonlocal elasticity theory. *Acta Mechanica Sinica*, *28*(3), pp.801-807.

Hahn, Thomas. 2007. "Cuba—a library for multidimensional numerical integration". *Computer Physics Communications.* 176 (11-12): 712-713.

Hosseini-Hashemi, S., Khorshidi, K. and Payandeh, H., 2009. Vibration analysis of moderately thick rectangular plates with internal line support using the Rayleigh-Ritz approach. *Scientia Iranica, Transaction B: Mechanical Engineering*, *16*(1), pp.22-39.

Ke, L.-L., Wang, Y.-S., Yang, J., Kitipornchai, S., 2014, Free vibration of size-dependent magneto-electro-elastic nanoplates based on the nonlocal theory. *Acta Mechanica Sinica.* 30 (4): 516-525.

Khodabakhshi, P., Reddy, J.N., 2015, A unified integro-differential nonlocal model". *International Journal of Engineering Science*. 95 (1): 60-75.

Khorshidi, K., Asgari, T. and Fallah, A., 2015. Free Vibrations Analysis of Functionally Graded Rectangular Nano-plates based on Nonlocal Exponential Shear Deformation Theory. *Mechanics of Advanced Composite Structures*, *2*(2), pp.79-93.

Khorshidi, K. and Bakhsheshy, A., 2015. Free vibration analysis of a functionally graded rectangular plate in contact with a bounded fluid. *Acta Mechanica*, *226*(10), p.3401.

Khorshidi, K. and Fallah, A., 2016. Buckling analysis of functionally graded rectangular nano-plate based on nonlocal exponential shear deformation theory. *International Journal of Mechanical Sciences*, *113*, pp.94-104.

Kröner, E., 1967, Elasticity theory of materials with long range cohesive forces. *International Journal of Solids and Structures*, 3(5), 731–742.

Krumhansl, J., 1968, Some considerations of the relation between solid state physics and generalized continuum mechanics. In E. Kröner (Ed.), *Mechanics of generalized continua*. IUTAM symposia (pp. 298–311). Berlin Heidelberg: Springer.

Kunin, I. A., 1968, The theory of elastic media with microstructure and the theory of dislocations. In E. Kröner (Ed.), *Mechanics of generalized continua*. IUTAM symposia (pp. 321–329). Berlin Heidelberg: Springer.

Lu, P., Zhang, P.Q., Lee, H.P., Wang, C.M., Reddy, J.N., 2007, Non-Local Elastic Plate Theories. *Proceedings of the Royal Society A: Mathematical, Physical and Engineering Sciences.* 463 (2088): 3225-3240.

Murmu, T., Pradhan, S.C., 2009, Vibration analysis of nanoplates under uniaxial prestressed conditions via nonlocal elasticity. *Journal of Applied Physics.* 106 (10): 104301.

Pisano, A.A., Fuschi, P., 2003, Closed form solution for a nonlocal elastic bar in tension. *International Journal of Solids and Structures*, 40(1), 13–23.

Pisano, A.A., Sofi, A., Fuschi, P., 2009a, Nonlocal integral elasticity: 2D finite element based solutions. *International Journal of Solids and Structures*, 46(21), 3836–3849.

Pisano, A.A., Sofi, A., Fuschi, P., 2009b, Finite element solutions for nonhomogeneous nonlocal elastic problems. *Mechanics Research Communications*. 36 (7): 755-761.

Polizzotto, C., 2001, Nonlocal elasticity and related variational principles. *International Journal of Solids and Structures*, 38(42–43), 7359–7380.

Reddy, J.N., 2004, Mechanics of laminated composite plates and shells: theory and analysis. Boca Raton: CRC Press.

Shaat, M., 2015, Iterative nonlocal elasticity for Kirchhoff plates. *International Journal of Mechanical Sciences.* 90: 162-170.

Thai, H.-T., Vo, T. P., Nguyen, T.-K., Lee, J., 2014, A nonlocal sinusoidal plate model for micro/nanoscale plates. *Proceedings of the Institution of Mechanical Engineers, Part C: Journal of Mechanical Engineering Science.* 228 (14): 2652-2660.

Wang, C.M., Kitipornchai, S., Lim, C.W., Eisenberger, M., 2008, Beam bending solutions based on nonlocal Timoshenko beam theory. *Journal of Engineering Mechanics*, 134(6), 475–481.

Appendix A

The coefficients C_{2p} and C_{3p} on the evolution function $h_p(\xi)$, for the cantilever case, are given by,

$$
\begin{gathered}
R_{0p} = \mathbb{X}_p(0), S_{0p} = \mathbb{X}_p'(0), R_{1p} = \mathbb{X}_p(1), S_{1p} = \mathbb{X}_p'(1) \\
C_{1p} = 0 \\
Q_{22} = 2S_{1p} + R_{1p} \\
Q_{23} = 3S_{1p} + 3R_{1p} \\
Q_{32} = S_{1p} \\
Q_{33} = 3S_{1p} + R_{1p} \\
\varphi_2 = -\left(4S_{1p} + 6R_{1p}\right) \\
\varphi_3 = -\left(6S_{1p} + 4R_{1p}\right) \\
C_{2p} = \frac{\varphi_2 Q_{33} - \varphi_3 Q_{23}}{Q_{22}Q_{33} - Q_{32}Q_{23}} \\
C_{3p} = \frac{\varphi_3 Q_{22} - \varphi_2 Q_{32}}{Q_{22}Q_{33} - Q_{32}Q_{23}}
\end{gathered}
\tag{A.1}
$$

Also, for the Free-Free case, the coefficients C_{1p}, C_{2p}, C_{3p} and C_{4p} on the evolution function $h_p(\xi)$ are obtained as follows,

$$
\begin{gathered}
R_{0p} = \mathbb{X}_p(0), S_{0p} = \mathbb{X}_p'(0), R_{1p} = \mathbb{X}_p(1), S_{1p} = \mathbb{X}_p'(1) \\
Q_{11} = R_{1p}^2 + R_{1p}S_{1p} + 0.5S_{1p}^2 \\
Q_{12} = 3R_{0p}^2 - 4R_{0p}S_{0p} + 3S_{0p}^2 \\
Q_{13} = R_{0p}^2 - 2R_{0p}S_{0p} + 2S_{0p}^2 \\
Q_{14} = R_{0p} - 1.5S_{0p} \\
Q_{41} = -5\left(4R_{1p}^2 + 5R_{1p}S_{1p} + 3S_{1p}^2\right) \\
Q_{42} = R_{1p}^2 + 2R_{1p}S_{1p} + 1.5S_{1p}^2 \\
Q_{43} = R_{1p} + S_{1p} \\
Q_{44} = 2\left(3R_{1p}^2 + 4R_{1p}S_{1p} + 3S_{1p}^2\right) \\
Q_{45} = R_{1p}^2 + 2R_{1p}S_{1p} + 2S_{1p}^2 \\
Q_{46} = R_{1p} + 1.5S_{1p} \\
\varphi_1 = R_{0p}^2 \\
\varphi_2 = R_{0p}S_{0p} \\
\varphi_3 = S_{0p}^2 \\
\varphi_4 = S_{1p}^2 \\
\varphi_5 = R_{1p}S_{1p} \\
\varphi_6 = R_{1p}^2 S_{0p} \\
\varphi_7 = R_{0p}^2 S_{1p} \\
C_{1p} = \frac{10Q_{11}\varphi_1}{2(-\varphi_6 Q_{14} + \varphi_5 Q_{13}) + \varphi_4 Q_{12}} \\
C_{2p} = -\frac{S_{0p}}{R_{0p}} C_{1p} \\
C_{3p} = -\frac{S_{0p}}{R_{0p}} C_{2p} \\
C_{4p} = \frac{10(-\varphi_7 Q_{43} + \varphi_2 Q_{42}) + \varphi_3 Q_{41}}{4(\varphi_7 Q_{46} - \varphi_2 Q_{45}) + \varphi_3 Q_{44}}
\end{gathered}
\tag{A.2}
$$

Graphical abstract